Springer Proceedings in Advanced Robotics 11
Series Editors: Bruno Siciliano · Oussama Khatib

Jing Xiao
Torsten Kröger
Oussama Khatib *Editors*

Proceedings of the 2018 International Symposium on Experimental Robotics

EXTRAS ONLINE

Springer

Springer Proceedings in Advanced Robotics 11

The Springer Proceedings in Advanced Robotics (SPAR) publishes new developments and advances in the fields of robotics research, rapidly and informally but with a high quality.

The intent is to cover all the technical contents, applications, and multidisciplinary aspects of robotics, embedded in the fields of Mechanical Engineering, Computer Science, Electrical Engineering, Mechatronics, Control, and Life Sciences, as well as the methodologies behind them.

The publications within the "Springer Proceedings in Advanced Robotics" are primarily proceedings and post-proceedings of important conferences, symposia and congresses. They cover significant recent developments in the field, both of a foundational and applicable character. Also considered for publication are edited monographs, contributed volumes and lecture notes of exceptionally high quality and interest.

An important characteristic feature of the series is the short publication time and world-wide distribution. This permits a rapid and broad dissemination of research results.

More information about this series at http://www.springer.com/series/15556

Jing Xiao · Torsten Kröger · Oussama Khatib
Editors

Proceedings of the 2018 International Symposium on Experimental Robotics

Springer

Editors
Jing Xiao
Robotics Engineering
Worcester Polytechnic Institute
Worcester, MA, USA

Torsten Kröger
Karlsruhe Institute of Technology
Karlsruhe, Baden-Württemberg, Germany

Oussama Khatib
Department of Computer Science
Stanford University
Stanford, CA, USA

ISSN 2511-1256 ISSN 2511-1264 (electronic)
Springer Proceedings in Advanced Robotics
ISBN 978-3-030-33949-4 ISBN 978-3-030-33950-0 (eBook)
https://doi.org/10.1007/978-3-030-33950-0

This Springer imprint is published by the registered company Springer Nature Switzerland AG
The registered company address is: Gewerbestrasse 11, 6330 Cham, Switzerland

Foreword

At the dawn of the century's third decade, robotics is reaching an elevated level of maturity and continues to benefit from the advances and innovations in its enabling technologies. These all are contributing to an unprecedented effort to bringing robots to human environment in hospitals and homes, factories and schools, in the field for robots fighting fires, making goods and products, picking fruits and watering the farmland, saving time and lives. Robots today hold the promise for making a considerable impact in a wide range of real-world applications from industrial manufacturing to health care, transportation, and exploration of the deep space and sea. Tomorrow, robots will become pervasive and touch upon many aspects of modern life.

The *Springer Tracts in Advanced Robotics (STAR)* was launched in 2002 with the goal of bringing to the research community the latest advances in the robotics field based on their significance and quality. During the latest fifteen years, the STAR series has featured publication of both monographs and edited collections. Among the latter, the proceedings of thematic symposia devoted to excellence in robotics research, such as ISRR, ISER, FSR, and WAFR, have been regularly included in STAR.

The expansion of our field as well as the emergence of new research areas has motivated us to enlarge the pool of proceedings in the STAR series in the past few years. This has ultimately led to launching a sister series in parallel to STAR. The *Springer Proceedings in Advanced Robotics (SPAR)* is dedicated to the timely dissemination of the latest research results presented in selected symposia and workshops.

This volume of the SPAR series brings the proceedings of the sixteenth edition of the International Symposium on Experimental Robotics (ISER). This symposium took place in Buenos Aires, Argentina, from November 5 to 8, 2018. The seven-part volume edited by Jing Xiao, Torsten Kröger, and Oussama Khatib is a collection of 67 contributions spanning a wide range of topics in robotics, including medical robotics, unmanned aerial vehicles, mobile robot navigation, mapping and localization, field robotics, robot learning, manipulation, human–robot interaction,

and design and prototyping. Experimental validation of algorithms, concepts, or techniques is the common thread running through this large research collection.

From its classical venue to its excellent program, the fifteenth edition of ISER culminates with this unique reference on the current developments and new directions of experimental robotics—a genuine tribute to its contributors and organizers!

July 2019

Bruno Siciliano
SPAR Editor

Preface

Experimental Robotics XVI is the collection of contributions presented at the 2018 International Symposium on Experimental Robotics (ISER 2018), November 5–8, 2018, Buenos Aires, Argentina. A total of 67 contributions were selected via peer review out of 120 submissions. The contributions cover a wide range of topics in robotics, including medical robotics, unmanned aerial vehicles, mobile robot navigation, mapping and localization, field robotics, robot learning, manipulation, human-robot interaction, and design and prototyping. The common emphasis is on experimental testing and validation of new ideas and methodologies, and this collection of contributions represents the latest in experimental research in robotics.

ISER is a series of biennial international symposia. Sponsored by the International Foundation of Robotics Research (IFRR), the goal of ISER symposia is providing a single-track forum for research in robotics that focuses on novelty of theoretical contributions validated by experimental results. Taking advantage of the small group setting, ISER 2018, for the first time, paired a discussion session with each regular session to better facilitate the exchange of ideas related to the session theme.

ISER 2018 also featured a pre-symposium workshop for outreach to robotics researchers and students in Argentina and surrounding countries and a post-symposium industrial forum to facilitate discussion of robotics applications and technology transfer. In doing so, ISER 2018 continued the unique tradition of ISER as an ambassador of robotics in the host country and region.

We thank all the reviewers for their important work in maintaining the high quality of the symposium. We also thank Franka Emika and the US National Science Foundation for providing financial support to the symposium or its participants. Most of all, we thank all the authors and participants for their technical contributions.

Jing Xiao
Torsten Kröger
Oussama Khatib

Contents

Micro Aerial Vehicles

Robot Learning I

Robot Navigation

Contacts and Manipulation

Unmanned Aerial Vehicles III

Human-Robot Interaction

Robot Design and Prototypes

Medical Robotics

Medical Robotics

Torsten Kroeger

All five papers of this session cover advancements for hardware and software components as well as algorithms that will improve or enable medical robotics applications. Niyaz *et al*. presented a motion planning concept validated by physical and simulated experiments, which allowed tentacle-like robots composed of pre-curved telescoping tubes to navigate through tissue. This would enable novel minimally invasive surgery applications requiring robot navigation in highly constraint spaces. The work of Kim *et al*. offered a comparable hardware setup and focused on non-surgical approaches to open narrowed coronary arteries and restore arterial blood flow to the heart tissue. Compared to the tentacle-like robots, the robots were wire-guided. The wires were tracked through fluoroscopy. Chitalia *et al*. introduced a new hardware design for robot joints for robotic pediatric neuroendoscopes – a tendon-driven continuum robot, which was feasible for use in the tip of neuroendoscopes. Wartenberg *et al*. presented a novel design of a six-degree-of-freedom system that could be used for needle insertion tasks inside of MRI scanning system. With the goal of modeling, understanding, and transferring human skills to robot devices, Chaudhari *et al*. discussed parameterizing musculoskeletal models with deep learning methods – an approach that offered the potential for future human-robot rehabilitation applications.

Given the current interest and growth in machine learning algorithms, most discussions during the discussion panel of this session were geared to data-driven modeling and engineering approaches. For instance, the panel and the audience discussed opportunities for using data-driven and model-free approaches for kinematic models of complex systems such as continuum robots.

Following Surgical Trajectories with Concentric Tube Robots via Nearest-Neighbor Graphs

Sherdil Niyaz[1(✉)], Alan Kuntz[2], Oren Salzman[3], Ron Alterovitz[2], and Siddhartha Srinivasa[1]

[1] School of Computer Science and Engineering, University of Washington, Seattle, USA
sniyaz@cs.washington.edu
[2] Department of Computer Science, University of North Carolina at Chapel Hill, Chapel Hill, USA
[3] The Robotics Institute, Carnegie Mellon University, Pittsburgh, USA

1 Introduction

Concentric tube robots, or CTRs, are tentacle-like robots composed of precurved telescoping tubes (Fig. 1a) and are controlled by rotating and translating each individual tube [6]. Their dexterity and small diameter enable minimally-invasive surgery in constrained areas, such as accessing the pituitary gland via the sinuses. Unfortunately, their unintuitive kinematics make manually guiding the tip while also avoiding obstacles with the entire tentacle-like shape extremely difficult [19]. This motivates a need for new user interfaces and planning algorithms.

Although existing planners [19] enable CTRs to reach specified points in task-space, this is often insufficient. For example, cutting a window in the skull during brain surgery (Fig. 1b) requires specifying an entire *path* R for the robot's tip. We have, to the best of our knowledge, implemented the first planner in this domain able to compute a trajectory that closely follows such a task-space path.

Algorithms that are able to follow some task-space path R by computing a constrained path in configuration space ($\mathcal{C}$-space) [2,14,17,22] have two main challenges: (i) some (e.g., a vector-field planner [17]) are fast but myopic, often falling into local minima and (ii) all are oblivious to how closely the generated paths follow R. In contrast, Holladay et al. [9] address both concerns by constructing a layered graph L in $\mathcal{C}$-space and searching it for a path that *directly* minimizes the Fréchet distance [21] from R.

Key to this algorithm's efficiency are the graph's ordered layers (Fig. 2a), each consisting of multiple Inverse Kinematics (IK) solutions for a specific point on R. Directed edges connect each configuration to others in the same and adjacent layers, ensuring monotonic progress. Unfortunately, this requires any path through

Electronic supplementary material The online version of this chapter (https://doi.org/10.1007/978-3-030-33950-0_1) contains supplementary material, which is available to authorized users.

J. Xiao et al. (Eds.): ISER 2018, SPAR 11, pp. 3–13, 2020.
https://doi.org/10.1007/978-3-030-33950-0_1

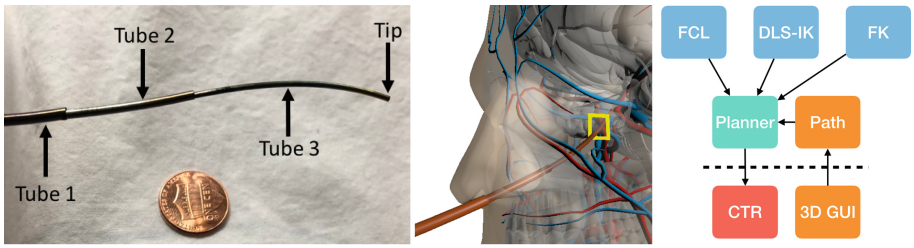

Fig. 1. (a) CTR with coin for scale. (b) Depiction of a CTR deployed via the sinus. A reference path R, used to cut a window in the skull with the CTR's tip, is depicted in yellow. (c) An example of a surgical system that uses our planner as a core component.

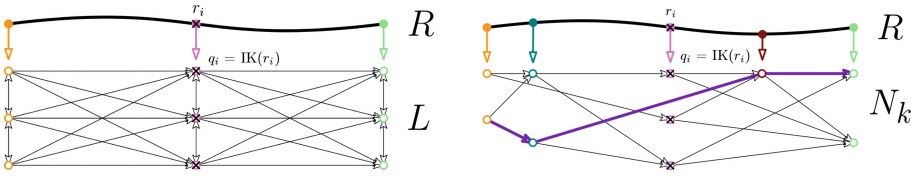

Fig. 2. (a) Layered graph L and (b) nearest-neighbor graph N_k constructed in $\mathcal{C}$-space to follow a reference path R in task-space. Note that a layer in L is depicted as a vertical stack of nodes. If reaching r_i is impossible, all paths in L become blocked. The structure of N_k, however, can bypass such blockages.

L to touch R at *every* layer, leading to failure in constrained environments such as ours. For example, a layer mapping to a point $r_i \in R$ made unreachable due to collisions causes no collision-free path to exist in the graph. The CTR's kinematics make it difficult for a surgeon specifying a path to perfectly distinguish feasible locations in task space, accentuating this failure mode.

Our key insight is to generalize this algorithm by searching over a *nearest-neighbor* graph, with less restrictive connections that allow deviation from infeasible portions of R (Fig. 2b). This makes planning in constrained anatomical environments possible, and thus enables our key contribution—a system implemented on a CTR, presented with a set of simulated and physical experiments. The former reveal that our planner produces higher-quality solutions more reliably than alternative algorithms, while the latter inform algorithmic next-steps necessary to bridge the simulation and real-robot gap.

2 Technical Approach

2.1 Notation and Definitions

The Fréchet distance is a metric of path similarity that has been extensively studied in computational geometry, with varied applications such as speech [12]

and handwriting [18] recognition. It can be explained intuitively via an analogy where a dog on a leash traverses one path while its owner traverses another, each with independent speed parameterizations α and β. In this case, the Fréchet distance is the shortest leash length required for the two to stay connected, assuming the dog and its owner are selecting optimal values of α and β.

Motion plans for surgical tasks, such as tissue manipulation, must respect the physician's intent by (i) minimizing the tip's deviation from the specified path at each point in time and (ii) following the "flow" of the path by ensuring that consecutive points along the two paths are traversed in the same order. Because the Fréchet distance captures both objectives, it provides an excellent optimization criteria for our domain.

Our planner searches for these motion plans in $\mathcal{C}$-space, the set of all possible configurations of the robot. Each configuration is a d-dimensional point that uniquely defines the robot's shape. Similarly, the task-space of the robot is defined as the space of all possible end-effector positions. We use the Forward Kinematics (FK) operator to map points in $\mathcal{C}$-space to points in task-space, and use the Inverse Kinematics (IK) operator to perform the reverse mapping.

For a CTR, a configuration must describe the translation ℓ_i and rotation θ_i of each individual tube. Thus, for a CTR comprised of k tubes (typically three or four), each configuration is a $2k$-length tuple $q = (\ell_1, \theta_1, \ldots, \ell_k, \theta_k)$. We define the robot's task-space as the $\mathbb{R}^3$ location of its tip, which is sufficient for many procedures such as cutting with heat or a laser. However, we note that our planner can easily be used with other definitions of task-space that also account for the tips's orientation.

In our setting, the physician specifies a reference path R in task-space as a sequence of $\mathbb{R}^3$ waypoints. Let Γ denote the set of collision-free $\mathcal{C}$-space paths and $\mathcal{F} : \mathbb{R}^3 \times \mathbb{R}^3 \to \mathbb{R}$ denote the discrete[1] Fréchet distance between two task-space paths. Our problem now calls for computing[2]

$$\arg\min_{\gamma \in \Gamma} \mathcal{F}(\mathrm{FK}(\gamma), R).$$

2.2 Algorithmic Approach

Recall that Holladay et al. [9] construct a layered graph L in $\mathcal{C}$-space. This is done by evenly sampling waypoints along the reference path R, and computing a "layer" of distinct IK solutions for each one. Each of these configurations has out-edges to all configurations in both the same and next immediate layer. Following Har-Peled and Raichel [8], the cross-product graph $\Phi = L \times R^3$ is

[1] Computing the continuous Fréchet distance, is notoriously difficult [16]. Thus, we use the *discrete* variant, easily computed using dynamic programming [5]. Here, the "leash" between points on the two paths is computed only for a discrete set of points and serves as an approximation of the (continous) Fréchet distance.

[2] By a slight abuse of notation we use FK to map both points as well as paths in $\mathcal{C}$-space to points and paths in task space, respectively.

[3] By a slight abuse of notation we treat R both as the discrete reference path as well as the one-dimensional graph defined by this sequence of waypoints.

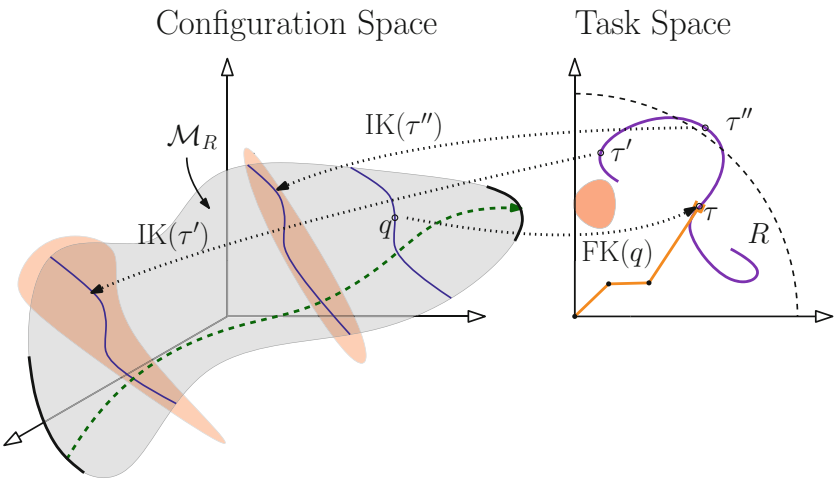

Fig. 3. A reference path R (purple, right) in the task-space of a robot (yellow, right) induces a manifold $\mathcal{M}_R$ of IK solutions in $\mathcal{C}$-space (grey, left). Following R via a layered graph requires traversing $\mathcal{M}_R$ from one end to the other, such as by taking the path in green. However, even if R is not directly in collision with some obstacle (red, right), its presence may cause a point $\tau' \in R$ to map to a self-manifold [3] IK(τ') that is completely in collision (red, left) given the kinematics of the robot. These in-collision self-manifolds require deviating from $\mathcal{M}_R$ to approximate R, and make traversal via the layered graph impossible.

then constructed and searched for a minimal-bottleneck path, which induces the path $\xi \in L$ such that FK(ξ) minimizes the discrete Fréchet distance with R.

Algorithmic Enhancement: Our early experiments, however, revealed that this planner often fails in surgical scenarios. In these constrained environments, some sampled waypoint $r_i \in R$ may be unreachable, often due to a combination of collisions and robot kinematics (Fig. 3). Even the existence of *one* such waypoint prevents the algorithm from finding any solutions, as all paths are blocked by a layer of configurations in collision (Fig. 2a). To prevent this, we construct a nearest-neighbor graph N_k by uniformly sampling IK solutions from R and connecting each to its k-nearest neighbors (NN) in $\mathcal{C}$-space. This less-rigid structure allows the planner to avoid IK solutions sampled from infeasible waypoints (Fig. 2b).

Specifically, each configuration q is connected to its k-NN in $Q_s(q)$, the set containing all $q_s \in N_k$ such that FK(q_s) lies after FK(q) along R. This ensures that any path through N_k monotonically follows R. As in [9], we generate the path $\xi \in N_k$ that minimizes the Fréchet distance with R by searching the cross-product graph $\Phi = N_k \times R$.

Densification: This graph-based approach allows solutions to be improved on-demand by sampling additional IK solutions from R and densifying N_k. To connect each newly-sampled solution q to N_k, we add out-edges from q to its

k-NN in $Q_s(q)$. In addition, we add in-edges to q from its k-NN in $Q_p(q)$, the set containing all $q_p \in N_k$ such that $\text{FK}(q_p)$ lies before $\text{FK}(q)$ along R. These additional connections increase the set of paths the planner can search over, while still constraining it to monotonically follow R.

Implementation details: We collision check edges lazily [4,7], using LPA* [11] for efficient replanning. Our CTR has three tubes, each of which can be rotated and translated, inducing a 6-dimensional $\mathcal{C}$-space. We use the damped least squares (DLS) IK algorithm [20], which has previously been used with the CTR [19]. We represent obstacles as polygonal meshes, and use FCL [13] for collision checks. We define the distance between two configurations q_1 and q_2 as:

$$\sum_k |\ell_{k1} - \ell_{k2}| + \rho(\theta_{k1}, \theta_{k2})$$

where ρ denotes the $SO(2)$ difference between two angles. We note that the choice of distance metric can drastically affect the algorithm's performance [1].

3 Experiments and Results

We consider four surgically-motivated reference paths in our experimental evaluation (Fig. 4), all within a human skull base. The first (i) moves the CTR's tip in a straight line towards the back of the sinuses, ending near a region where the second (ii) traces a trapezoid. These two paths are inspired by a clinical scenario where the CTR is deployed via the first path, and then uses the second to cut a window allowing deeper access into the skull. We also test (iii) a different version of the second path, as well as (iv) a W-shaped path that could be used for wound irrigation. While not in collision with the skull, these last two paths reside in constrained areas and thus exhibit the phenomenon depicted in Fig. 3.

3.1 Simulation Comparison

We evaluate our algorithm, which we term NN Graph, in simulation and compare its performance with the following alternatives: (a) VFP which follows a vector-field along R by using the Jacobian to integrate a path in $\mathcal{C}$-space [17], (b) GreedyIK which adaptively samples a set of ordered IK solutions from R

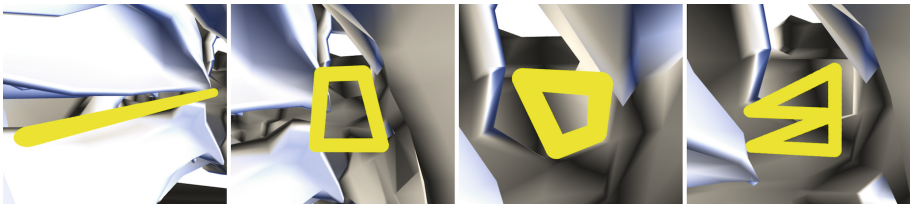

Fig. 4. From left to right, reference paths (i) through (iv) used in our experiments.

and attempts to interpolate a collision-free path in $\mathcal{C}$-space between them [17], (c) CBiRRT which enables planning on constraint manifolds [2] and (d) Layered Graph—the approach presented by Holladay et al. [9]. It is worth noting that planners (a) and (b) are myopic but efficient and that all but (d) were not designed to minimize the Fréchet distance from a reference path.

Simple Paths: We first compare the planners using paths (i) and (ii), both without regions made unreachable by the collision geometry or CTR kinematics. We report the Fréchet distances of the produced trajectories from R for a wide set of parameters (Fig. 5) and average results over ten random seeds.

We see that for both paths, all planners successfully produce solutions. When using path (i), a straight line, performance for all planners remains fairly stable as parameters vary. However, both paths reveal weaknesses in VFP and GreedyIK. With the former, optimal performance on path (ii) is only achieved under two sets of parameters. Similarly, GreedyIK produces results of markedly lower quality than NN Graph across most parameters. CBiRRT, meanwhile, is used to pin the CTR's tip within a tolerance of R and succeeds when this tolerance is made sufficiently tight. This is especially evident on path (i), the straight line.

Constrained Paths: We also compare the planners using paths (iii) and (iv), as seen in Fig. 6. Due to being located in constrained areas, these paths contain small regions infeasible for the CTR to follow perfectly. We note that these paths were not hand-engineered adversarially, but were generated by a human familiar with the CTR and real-world surgical procedures.

Due to the infeasible regions, Layered Graph was unable to find any solutions with either path, confirming the failure mode we observed in our early experiments. While CBiRRT still constrains the CTR's tip to lie within a tolerance of R, it lacks any notion of path following, causing it to violate the flow of these more constrained paths. This oblivious nature also hinders GreedyIK, causing it to display unstable behavior where sampling *more* IK solutions can cause a sharp drop in solution quality.

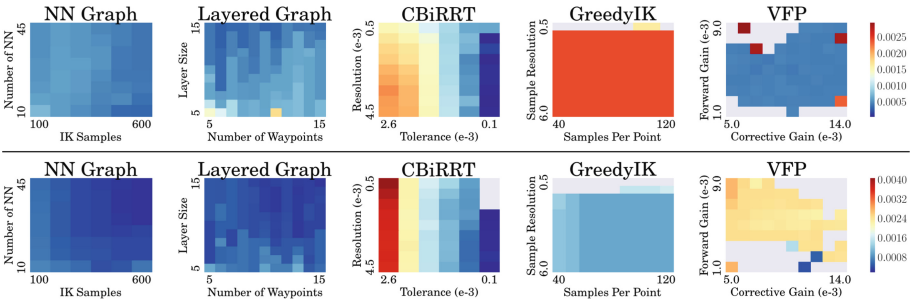

Fig. 5. Fréchet distances over a range of parameters for path (i) at top and path (ii) at bottom. A grey square indicates the algorithm failed to find a solution with that combination of parameters.

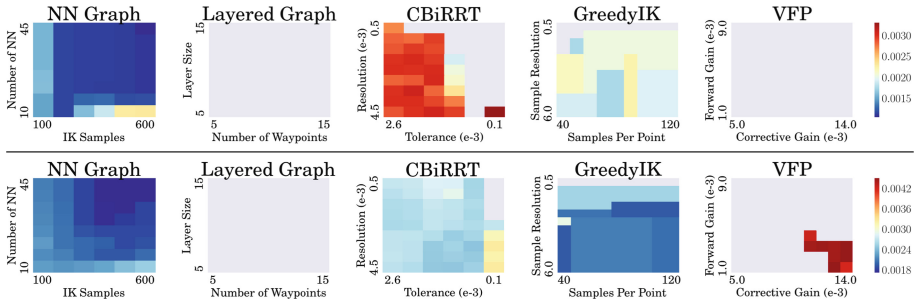

Fig. 6. Fréchet distances for path (iii) at top and path (iv) at bottom. We note that Layered Graph failed on both paths, and that VFP failed on path (iii).

In our experiments with all four paths, NN Graph displayed stable behavior under parameter variation and was the only planner able to consistently produce high-quality solutions. In fact, for each of the four other planners, at least one path led to either very low quality solutions or no solutions being found.

Additional Comparisons: We use our results from path (iii) to perform additional comparisons between planners. In the first of these, we correlate Fréchet distance and runtime for each planner by averaging results across all parameters over ten-second windows (Fig. 7a). This confirms that GreedyIK produces solutions quickly due to its simple nature. However, our planner outperforms the others, which display fluctuating behavior over time.

In addition to evaluating our planner over a range of parameters, we are interested in how a *single* set of parameters generalizes across a range of reference paths. We compare against GreedyIK using its optimal parameters, and select a set for NN Graph that lead to similar runtime on path (iii). Generalization is evaluated by adding independent Gaussian noise to the corners defining this path and recording planner success rates (each taken over 20 trials) under increasing levels of noise (Fig. 7b). We see that as the level of noise increases, our planner has a higher success rate than GreedyIK.

3.2 Algorithmic Behavior

Runtime Analysis: A decomposition of NN Graph's runtime on path (iii) as we linearly scale both the number of nearest-neighbors and IK solutions sampled is shown in Fig. 7c. FK, used in constructing the nodes of the cross-product graph Φ [8,9], is notably the most expensive component. This cost arises from modeling complex interactions between tubes, which requires solving a series of differential equations rather than the typical matrix multiplication.

Densification: We also explore the ability of densification to improve existing NN Graph solutions. This provides our planner an advantage over alternatives, as it enables a physician to improve a solution online until they are satisfied. Our

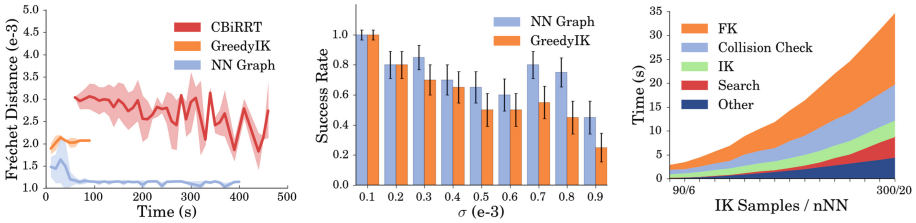

(a) Fréchet vs. Time (b) Robustness to Noise (c) Runtime Components

Fig. 7. (a) Fréchet distance as a function of the runtime for each planner. (b) Success rates for NN Graph and GreedyIK as we inject more noise into R. (c) A decomposition of the runtime of our NN Graph. All results use path (iii)

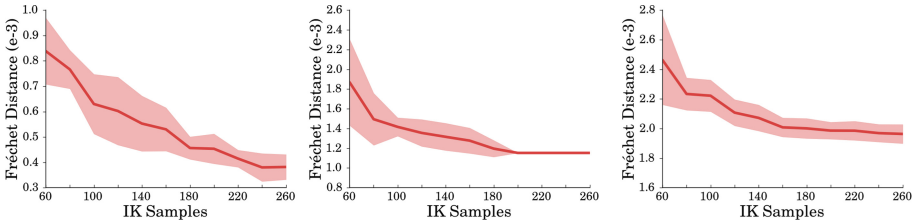

(a) Path (ii) (b) Path (iii) (c) Path (iv)

Fig. 8. Densification results.

trials use 20 nearest-neighbors and augment N_k with an additional 20 configurations per densification iteration. We report the Fréchet distances of solutions as the graph increases in size.

Densification provides very little improvement with path (i), likely because this simple straight-line path makes the initial solution already close to optimal. The other three paths display notable improvement as the size of N_k increases (Fig. 8). However, paths (iii) and (iv) both exhibit diminishing returns past a given iteration.

3.3 Physical Experiments

We evaluate our algorithm on the real robot, testing all four paths inside a 3D-printed model of the skull base anatomy. Parameters are selected that create high-quality solutions in simulation. To measure Fréchet distance, we use a magnetic tracking system to localize the tip during execution. Because this system is noisy, we execute each trajectory ten times and average the results.

Imperfections in our kinematic model (discussed in the next section) prevent us from scoring path (iii) due to collisions. While this path was not executed successfully, the other three were. Paths (iv), (ii), and (i) were each executed with average real Fréchet errors of 0.00806, 0.00747, and 0.00744 m respectively. These are all significantly higher than the respective simulation errors of 0.00211,

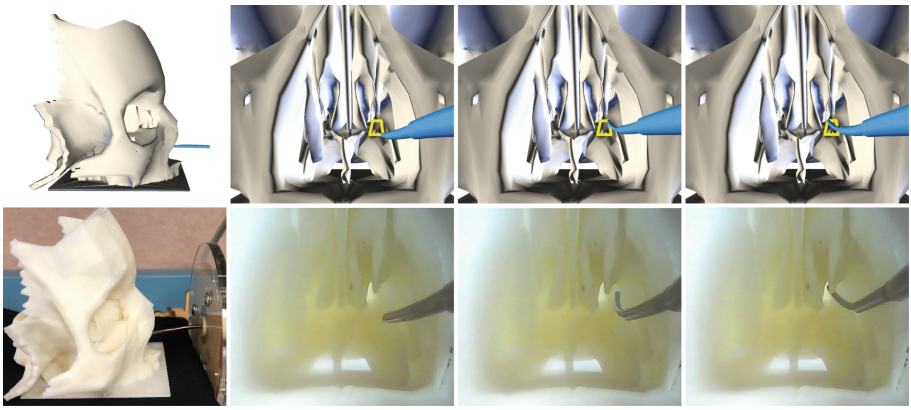

Fig. 9. Simulated (top) and real (bottom) execution of path (ii). The reference path is colored yellow in simulation.

0.00031, and 0.00034 m. This discrepancy arises primarily from the inaccuracies in our kinematic model. A comparison of simulated and real execution using path (ii) is shown in Fig. 9.

4 Experimental Insights and Future Work

Our experiments support our use of a nearest-neighbor graph and demonstrate the advantages of our planner over alternatives. They also reveal previously unconsidered domain-specific challenges, which we can only now begin to address. We propose solutions to each of these, which we will explore in future work.

Our planner's high runtime is mainly due to our robot's expensive FK (Fig. 7c), motivating a paradigm shift in planner design for all robots that incur high cost in this operation. To address this, we propose constructing the cross-product graph Φ implicitly, which avoids unnecessarily invoking FK to create nodes never expanded during the search.

While we demonstrate a successful planner, our physical experiments reveal the kinematic model has now become the limiting factor. Although this model is state-of-the-art [15], it fails to perfectly model certain physical phenomenon, such as friction between tubes. This causes the shape of the robot in simulation to only approximate reality. Naturally, improving this model is a solution. We also propose taking its uncertainty into account via a bicriteria optimization problem of (i) minimizing Fréchet and (ii) maximizing the distance of the robot from obstacles to prevent collisions. This has the added benefit of mitigating error in the collision geometry, constructed from a preoperative volumetric scan [10].

Additionally, successful execution of path (ii) on the real CTR required manually tuning the insertion point of the robot into the skull. The kinematics of the robot induce a trumpet-shaped workspace, leading to greater range of motion

farther from this insertion point. One of the insertion points was too close to the reference path, placing it outside the robot's workspace and causing a planning failure. Likewise, the successful insertion point placed the shaft of the robot in a less-constrained area, preventing a collision that otherwise occurred due to modeling error. Because it proved so consequential, we propose incorporating this selection of insertion point as a planning subproblem.

Acknowledgments. We thank Bob Webster and his group at Vanderbilt University for numerous discussions on CTRs and for creating the CTR used here. We thank Rachel Holladay for her invaluable insight in discussing her previous work. This work was (partially) funded by the National Institute of Health R01 (#R01EB019335), National Science Foundation CPS (#1544797), National Science Foundation NRI (#1637748), National Science Foundation RI Award 1149965, the Office of Naval Research, the RCTA, Amazon, and Honda.

References

1. Atias, A., Solovey, K., Salzman, O., Halperin, D.: Effective metrics for multi-robot motion-planning. CoRR, abs/1705.10300 (2017)
2. Berenson, D., Srinivasa, S., Ferguson, D., Kuffner, J.: Manipulation planning on constraint manifolds. In: ICRA, pp. 625–632 (2009)
3. Burdick, J.: On the inverse kinematics of redundant manipulators: characterization of the self-motion manifolds. In: ICRA, pp. 264–270 (1989)
4. Dellin, C., Srinivasa, S.: A unifying formalism for shortest path problems with expensive edge evaluations via lazy best-first search over paths with edge selectors. In: ICAPS, pp. 459–467 (2016)
5. Eiter, T., Mannila, H.: Computing discrete Fréchet distance. Technical report, Citeseer (1994)
6. Gilbert, H., Rucker, D., Webster III, R.J.: Concentric tube robots: the state of the art and future directions. In: ISRR, pp. 253–269 (2013)
7. Haghtalab, N., Mackenzie, S., Procaccia, A., Salzman, O., Srinivasa, S.: The provable virtue of laziness in motion planning. In: ICAPS, pp. 106–113 (2018)
8. Har-Peled, S., Raichel, B.: The Frećhet distance revisited and extended. TALG **10**(1), 3 (2014)
9. Holladay, R., Salzman, O., Srinivasa, S.: Minimizing task space Frećhet error via efficient incremental graph search. CoRR, abs/1710.06738 (2017)
10. Johnson, H., McCormick, M., Ibanez, L.: The ITK Software Guide Book 1: Introduction and Development Guidelines, vol. 1. Kitware Inc., New York (2015)
11. Koenig, S., Likhachev, M., Furcy, D.: Lifelong planning A*. Artif. Intell. **155**(1–2), 93–146 (2004)
12. Kwong, S., He, Q.H., Man, K.F., Tang, K.S., Chau, C.W.: Parallel genetic-based hybrid pattern matching algorithm for isolated word recognition. Int. J. Pattern Recogn. Artif. Intell. **12**(05), 573–594 (1998)
13. Pan, J., Chitta, S., Manocha, D.: FCL: a general purpose library for collision and proximity queries. In: ICRA, pp. 3859–3866 (2012)
14. ROS Industrial. Descartes (2015). Accessed 20 Apr 2018
15. Rucker, D.: The mechanics of continuum robots: model-based sensing and control. Ph.D. thesis, Vanderbilt University (2011)

16. Solovey, K., Halperin, D.: Sampling-based bottleneck pathfinding with applications to Fréchet matching. In: European Symposium on Algorithms, ESA, pp. 76:1–76:16 (2016)
17. Srinivasa, S., Johnson, A., Lee, G., Koval, M., Choudhury, S., King, J., Dellin, C., Harding, M., Butterworth, D., Velagapudi, P., Thackston, A.: A system for multi-step mobile manipulation: architecture, algorithms, and experiments. In: ISER, pp. 254–265 (2016)
18. Sriraghavendra, E., Karthik, K., Bhattacharyya, C.: Fréchet distance based approach for searching online handwritten documents. In: Document Analysis and Recognition, vol. 1, pp. 461–465. IEEE (2007)
19. Torres, L., Kuntz, A., Gilbert, H., Swaney, P., Hendrick, R., Webster III, R.J., Alterovitz, R.: A motion planning approach to automatic obstacle avoidance during concentric tube robot teleoperation. In: ICRA, pp. 2361–2367 (2015)
20. Wampler, C.: Manipulator inverse kinematic solutions based on vector formulations and damped least-squares methods. IEEE Trans. Syst. Man Cybern. **16**, 93–101 (1986)
21. Wylie, T., et al.: The discrete Fréchet distance with applications. Ph.D. thesis, Montana State University-Bozeman, College of Engineering (2013)
22. Yao, Z., Gupta, K.: Path planning with general end-effector constraints: using task space to guide configuration space search. In: IROS, pp. 1875–1880 (2005)

An Experimental Validation of Behavior-Based Motions for Robotic Coronary Guidewire Crossing Techniques

Young-Ho Kim(✉), Ankur Kapoor, Rodolfo Finocchi, and Erin Girard

Siemens Healthineers, Medical Imaging Technologies, Princeton, NJ, USA
{young-ho.kim,ankur.kapoor,rodolfo.finocchi,
erin.girard}@siemens-healthineers.com

Abstract. Percutaneous Coronary Intervention (PCI) is a non-surgical approach used to open narrowed coronary arteries and restore arterial blood flow to heart tissue. During a PCI procedure, the clinician uses X-ray fluoroscopy to visualize and guide the catheter, guidewire, and other devices (e.g. angioplasty balloons and stents). Robot-assisted PCI could potentially reduce the radiation exposure of operators and provide a more ergonomic workflow. However, modeling and controlling of the guidewire remains challenging because of the interplay of guidewire motions, the tip properties (e.g., loads, coating), and the local cross-sectional area of the vessel lumen (e.g, stenosis) and results in a highly non-linear system. Thus, robot-assisted PCI devices are still passively controlled by human operators at the cockpit. In this paper, we introduce methods to generate distal guidewire motions that take advantage of the fast response of a robotic system and which may be difficult to generate by a human hand. The fundamental motions that a robot can use to control the movement and direction of the guidewire are rotation and pushing/retracting, from the proximal end of the guidewire outside the insertion point on the patient's body. We begin by investigating combinations of these fundamental motions under structured environmental settings and conduct a systematic empirical comparison of task completion time for a given setting. We then demonstrate improved dynamic behavior motions for a soft guidewire, which shows a promising speed-up by 33% and 44% for two difficult stenosis cases.

Keywords: Robot-assisted PCI · Guidewire navigation · Behavior-based control · High-speed dynamic motion · Medical robots

Electronic supplementary material The online version of this chapter (https://doi.org/10.1007/978-3-030-33950-0_2) contains supplementary material, which is available to authorized users.

J. Xiao et al. (Eds.): ISER 2018, SPAR 11, pp. 14–23, 2020.
https://doi.org/10.1007/978-3-030-33950-0_2

1 Introduction

Percutaneous Coronary Intervention (PCI) [1] is a minimally invasive approach used to open coronary arteries that have been narrowed or blocked by atherosclerosis. During a PCI procedure, X-ray fluoroscopy is the primary imaging modality used to visualize and guide the catheter, guidewire, and other devices (*e.g.* angioplasty balloons and stents). The clinician is continuously exposed to X-rays while manipulating a guidewire through the catheter, into the coronary, and across the stenosis or blockage. Moreover, in order to reduce the degree of longterm radiation exposure, the interventional cardiologist wears a heavy lead apron during the entire procedure. To alleviate these workflow conditions and allow the clinician to sit on an ergonomic console, robots have been introduced [2] to remotely manipulate the guidewire and the catheter. However, they are still passively controlled by human operators at the cockpit. Modeling and controlling of the guidewire remains challenging because of the interplay of guidewire motions, the tip properties (*e.g.,* loads, coating), and the local cross-sectional area of the vessel lumen (*e.g,* stenosis) and results in a highly non-linear system. For the task of controlling guidewires to cross stenosed lesions, referred to as *wiring a vessel*, it is ideal to use as soft a wire as possible. A softer wire is likely to cause less damage to the vessel lumen and is less likely to result in adverse events, such a vessel perforations. During the procedure, clinicians often change to stiffer wires to cross a difficult stenosis and then switch back to a softer wire. A system that can combine the benefits of environmental modeling and *optimal* guidewire manipulation with human operator control could potentially reduce task completion time and allow the clinician to cross the stenosis without switching wires.

In this paper, we introduce methods to generate distal guidewire motions that take advantage of the fast response of a robotic system and which may be difficult to generate by a human hand. The fundamental motions that a robot can use to control the movement and direction of the guidewire are limited to rotation about its axis and pushing/retracting at the proximal end of the guidewire. We begin by investigating combinations of these fundamental motions under structured environmental settings and conduct a systematic empirical comparison of task completion time for a given setting. We then demonstrate improved dynamic behavior motions for soft guidewires on difficult stenosis cases.

1.1 Related Work

A detailed assessment of the mechanical properties of wires used in PCI is described by Schröder [3]. Guidance on various crossing techniques, wire selection and manipulation based on environmental conditions for the manual operator are described in [1,4,5]. Prior efforts at kinematics and dynamics modeling, including simulating wires [6–11], were directed at developing training simulators for physicians. In this work we focus on dynamic behavior motions and their interactions with the environment to assist the operator in crossing a stenosis with the softest wire possible.